Potential of Noninvasive Serial Assessment of Acute Renal Allograft Rejection by ^{18}F-FDG PET to Monitor Treatment Efficiency

Stefan Reuter*[1], Uta Schnöckel*[2], Bayram Edemir[1], Rita Schröter[1], Dominik Kentrup[1], Hermann Pavenstädt[1], Otmar Schober[2], Eberhard Schlatter[1], Gert Gabriëls[1], and Michael Schäfers[3]

[1]Department of Medicine D, Experimental Nephrology, University of Münster, Münster, Germany; [2]Department of Nuclear Medicine, University of Münster, Münster, Germany; and [3]European Institute for Molecular Imaging; University of Münster, Münster, Germany

We propose ^{18}F-FDG PET as a method to monitor acute rejection of allogeneic renal transplants in a rat model. **Methods:** Allogeneically transplanted (aTX) rats (binephrectomized Lewis–brown Norway to Lewis) served as the renal transplant model. aTX rats treated with cyclosporine A (CSA) served as a therapy monitoring group. Healthy control rats, rats with acute CSA nephrotoxicity, rats with acute tubular necrosis, syngeneically transplanted (sTX) rats, and aTX rats treated with CSA since postoperative day 0 served as controls. After surgery, renal glucose metabolism was assessed in vivo serially up to postoperative day 7 by performing small-animal PET 3 h after intravenous injection of 30 MBq of ^{18}F-FDG. Mean radioactivity (cps/mm^3 of tissue) was measured and the percentage injected dose calculated. Results were confirmed by histologic, functional, and autoradiographic analysis. **Results:** Renal ^{18}F-FDG uptake was significantly elevated at postoperative day 4 in aTX rats, when compared with control, sTX, acute tubular necrosis, or CSA-treated rats ($P < 0.05$). In vivo ^{18}F-FDG uptake correlated with the results of autoradiography and with inflammatory infiltrates observed on histologic examination. Notably, ^{18}F-FDG PET assessed the response to therapy 48 h earlier than the time at which serum creatinine decreased and when histologic examination still showed signs of allograft rejection. In aTX rats, the CSA-susceptible graft infiltrate was dominated by activated cytotoxic T cells and monocytes/macrophages. **Conclusion:** ^{18}F-FDG PET is an option to noninvasively assess early response to therapy in rat renal allograft rejection.

Key Words: renal transplantation; acute rejection; ^{18}F-FDG PET

J Nucl Med 2010; 51:1644–1652
DOI: 10.2967/jnumed.110.078550

Episodes of acute allograft rejection are a negative prognostic factor for the development of interstitial fibrosis and tubular atrophy—the morphologic surrogate of chronic renal allograft deterioration—and for long-term graft survival (*1–3*). The impact of allograft rejection on chronic renal allograft failure as the main cause for death-censored graft loss after kidney transplantation increases, whereas the severity of episodes itself is an independent risk factor (*2,4–6*). Hence, early detection and treatment of allograft rejection are crucial to limit the inflammatory process and preserve the function of the transplant. Standard care includes monitoring nonspecific signs of rejection, such as arterial hypertension, proteinuria, edema, graft tenderness, and changes in diuresis; monitoring serum parameters, such as creatinine, blood urea nitrogen (BUN), and cystatin c; and performing biopsy, still the gold standard in rejection diagnostics on allograft dysfunction (*7,8*). More than 50% of the rejection episodes are subclinical, without acute impaired renal function, whereas their histologic severity is not different from that of patients with a decrease in glomerular filtration rate during the acute rejection episode (*9*). Therefore, some authors suggest performing protocol biopsies at a defined time course after transplantation, irrespective of the status of graft function (*8*). As an invasive procedure, biopsy carries the risk of significant graft injury and is not feasible in patients taking anticoagulant medication (*10,11*). Moreover, the limited sampling sites (randomly chosen, and exceedingly small, portions of tissue) may lead to false-negative results, such as when rejection is focal or patchy.

At present, therapy response is monitored by assessing clinical parameters such as serum creatinine and BUN or changes in diuresis or edema. These parameters are rather unspecific; for example, up to 54% of patients with allograft rejection do not present with clinical signs, and these occur only later (*12,13*). Thus, therapy escalation or a switch to a more effective therapeutic regimen, as in the case of steroid-refractory rejection (usually not diagnosed until 3 d after the start of an immunosuppressant bolus regimen), might be delayed and lead to graft failure (*12,14*).

^{18}F-FDG PET is a noninvasive tool widely used for detecting, staging, and following up tumors, infections, and sterile inflammation (*15*). Recently, using a uninephrectomized rat renal transplant model, we established ^{18}F-FDG PET as an entirely image-based method to assess

Received May 3, 2010; revision accepted Jul. 14, 2010.
For correspondence or reprints contact: Stefan Reuter, Medizinische Klinik und Poliklinik D, Albert Schweitzer Strasse 33, D 48149 Münster, Germany.
E-mail: sreuter@uni-muenster.de
*Contributed equally to this work.

acute renal rejection (*16*). Recruited activated leukocytes within the graft undergoing rejection (*17,18*) lead to a local increase in metabolic activity visualized and measured by accumulation of ^{18}F-FDG (*16*). However, no studies have yet established ^{18}F-FDG PET for the early detection and follow-up of therapy response (immunosuppressive treatment efficacy) in renal allograft rejection.

Here, we applied ^{18}F-FDG PET in a renal transplant model using binephrectomized rats, mimicking the clinical situation more closely by the absence of the healthy native kidney that is present in uninephrectomized transplant models. Thus, impairment of kidney function results in disturbance of functional parameters, such as electrolyte–water homeostasis or azotemia. ^{18}F-FDG uptake in renal parenchyma was assessed on 4 postoperative days in allogeneically transplanted (aTX) animals with and without immunosuppressive therapy. The aim of the study was to evaluate ^{18}F-FDG PET as a method of monitoring response to therapy for acute renal transplant rejection in rats.

MATERIALS AND METHODS

Detailed methods are given in the supplemental materials (available online only at http://jnm.snmjournals.org).

Animal Models

Surgical and imaging experiments were approved by a governmental committee on animal welfare and were performed in accordance with national animal protection guidelines. We used male Lewis–brown Norway rats and male Lewis rats (200–270 g in body weight; Charles River) with free access to standard rat chow (Ssniff) and tap water. Transplantations were performed immediately after bilateral nephrectomy of the recipient. Grafts were recovered on postoperative day 1, 4, or 7 after transplantation. The chosen aTX model leads to histologic and functional changes typical of acute rejection (*19,20*). Syngeneically transplanted (sTX) rats (Lewis–brown Norway to Lewis–brown Norway) and aTX rats treated with cyclosporine A (CSA, 5 mg/kg of body weight/d intraperitoneally) since transplantation (postoperative day 0) without allograft rejection served as controls. Because acute tubular necrosis (ATN) and acute CSA toxicity are common differential diagnoses of allograft rejection, groups with these conditions were also included. ATN (as ischemia–reperfusion injury) and acute CSA toxicity were induced as described previously (*16,21*). Blood samples for analyses of creatinine and BUN were collected by tail vein puncture.

PET Image Acquisition

Images of nonfasting subjects were acquired as described previously (*16*). In short, ^{18}F-FDG uptake was calculated from a whole-body acquisition 30 min long at 3 h after injection of ^{18}F-FDG (30 MBq in 100 μL of 0.9% NaCl solution) into a tail vein of nonanesthetized rats. To minimize tracer uptake in the kidneys caused by renal excretion of ^{18}F-FDG, we started the acquisitions 3 h after ^{18}F-FDG injection. During the acquisition, the rats were anesthetized with oxygen/isoflurane inhalation (0.7 L of oxygen per minute/2% isoflurane), and body temperature was maintained at physiologic values by a heating pad. PET was performed with a high-resolution, multiwire, chamber-based small-animal camera (quadHIDAC; Oxford Positron Systems Ltd.) (*22*). To delineate the kidney contours, the ^{18}F-FDG PET acquisition was followed by intravenous injection of 5 MBq of ^{18}F-fluoride without moving the rat in the scanner and another PET acquisition 15 min in length.

PET Image Analysis and Quantitative Evaluation

Images were reconstructed into an image volume of 280 × 120 mm and a voxel size of 0.8 × 0.8 × 0.8 mm, using a list-mode–based resolution recovery reconstruction algorithm with no attenuation or scatter correction applied (*23*). A renal parenchyma volume of interest was manually traced around the kidneys on 12 reconstructed images 2 min after ^{18}F-fluoride injection. This volume of interest was projected onto the ^{18}F-FDG images. The renal pelvis was carefully excluded from the volume of interest to ensure that no renally excreted activity was included. Mean ^{18}F-FDG uptake in the renal parenchyma was calculated by the ratio of total counts to volume.

Autoradiography

To validate the ^{18}F-FDG PET uptake, we sacrificed the animals and harvested the kidneys immediately after ^{18}F-FDG scanning on postoperative day 4 or 7. High-resolution autoradiography (μ-imager; Biospace Measures) was performed as described previously (*16*).

Histology

Portions of the kidneys were snap-frozen and fixed in 4% formaldehyde in phosphate-buffered saline. We quantified the renal infiltration according to the total-inflammation (ti) score in the renal cortex (Supplemental Table 1), recently added to the Banff classification (*24*). The cortex was chosen because the extent of medullary inflammation does not reflect the degree of allograft rejection (*25*).

Real-Time Polymerase Chain Reaction (PCR)

Expression profiles of selected marker genes for infiltrating cells were validated by real-time PCR, which was performed using SYBR Green PCR Master Mix (Applied Biosystems) or TaqMan Universal PCR Master Mix (Applied Biosystems) on an ABI Prism 7700 sequence detection system (Applied Biosystems). Specific primer pairs were used (Supplemental Table 2). Relative gene expression was evaluated with the $2^{-\Delta\Delta Ct}$ method using glyceraldehyde 3-phosphate dehydrogenase as a housekeeping gene (*26*).

Statistics

Laboratory data were compared by ANOVA with a Bonferroni multiple-comparisons test. Data are presented as mean values ± SEM (n = number of rats, samples, or experiments). Significance was inferred at the $P < 0.05$ level.

RESULTS

Analysis of PET Images and Quantitative Evaluation

In allografts undergoing rejection, we detected a clearly elevated ^{18}F-FDG uptake, which was absent in kidneys without allograft rejection (Fig. 1). An example treatment-response experiment is presented in Figure 2. On postoperative day 4, the allograft was clearly seen on ^{18}F-FDG PET. Notably, only 24 h after commencement of CSA therapy, the ^{18}F-FDG signal of the graft had nearly disappeared. On the 2 following days, ^{18}F-FDG uptake in the allograft remained low when we used our previously introduced calculated percentage of ^{18}F-FDG activity (percentage injected dose,

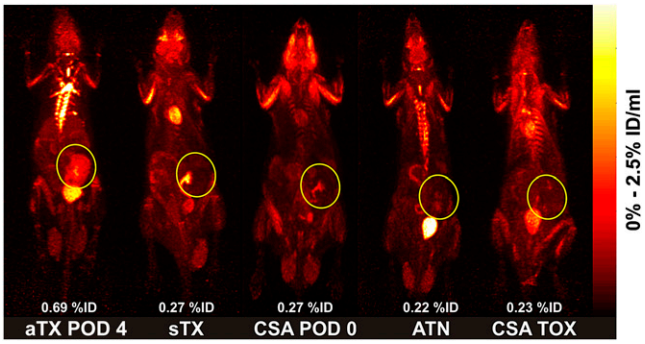

FIGURE 1. Representative PET images (day 4 after surgery) of static whole-body acquisitions of aTX rat, sTX rat, aTX rat treated daily with CSA (5 mg/kg intraperitoneally) starting on postoperative day 0, rat with ATN (ischemia–reperfusion injury), and rat with acute CSA nephrotoxicity (50 mg/kg for 2 d intraperitoneally) after tail vein injection of 30 MBq of ^{18}F-FDG (maximum a posteriori projection, whole-body acquisition for 30 min at 180 min after injection). Although parenchyma of renal allograft with acute rejection (aTX rats) accumulates ^{18}F-FDG, transplants of different control groups do not show significant accumulation. Renal pelvis—because it can contain eliminated ^{18}F-FDG—was excluded from measurements. Renal grafts are marked with yellow circles. %ID values are fraction of ^{18}F-FDG uptake in renal parenchyma. POD = postoperative day; TOX = nephrotoxicity.

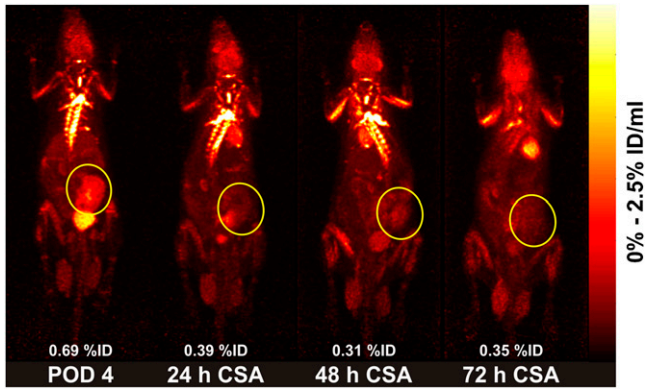

FIGURE 2. Series of representative PET images of static whole-body acquisitions (intravenous injection of 30 MBq of ^{18}F-FDG (maximum a posteriori projection, whole-body acquisition for 30 min at 180 min after injection) of aTX rat starting 4 d after transplantation. After development of acute rejection (allograft shows intense ^{18}F-FDG uptake on postoperative day 4), recipient was treated with CSA, 5 mg/kg/d intraperitoneally, and at 24 h after commencement of immunosuppressive therapy already showed significantly decreased ^{18}F-FDG uptake in renal parenchyma (≙ therapy response). Renal pelvis—because it can contain eliminated ^{18}F-FDG—was excluded from measurements. Renal graft is marked with yellow circles. %ID values are fraction of ^{18}F-FDG uptake in renal parenchyma. POD = postoperative day.

or %ID) within the parenchyma of the investigated kidney (*16*). Timelines of the %ID of ^{18}F-FDG measured in kidneys by PET are given in Figure 3. Kidneys developing allograft rejection (aTX rats) showed significantly increased ^{18}F-FDG uptake starting on postoperative day 4, when compared with all other models. No differences were found between controls, sTX rats, CSA-treated rats with and without acute CSA nephrotoxicity, and kidneys with ischemia–reperfusion injury. Notably, 1 d after commencement of immunosuppressive therapy, the ^{18}F-FDG uptake of grafts with former rejection already had significantly decreased and was no longer different from controls.

Autoradiography

Assessment of inflamed tissue by autoradiography (reference method to validate ^{18}F-FDG PET results) confirmed that ^{18}F-FDG accumulation correlated with the degree of infiltration (*27*). In our previous study, we showed that allograft ^{18}F-FDG uptake was 7-fold higher than uptake in controls. Postoperative day 4 was chosen for autoradiography because ^{18}F-FDG PET uptake in allografts reached significance at that time, when the integrity of the graft was still warranted. On postoperative day 4, aTX rats presented with a strong, cortex-accentuated, heterogeneous density distribution on autoradiography. In comparison, all other kidneys exhibited a faint and homogeneous density distribution with accentuation of the medulla (examples are presented in Fig. 4). This is the regular ^{18}F-FDG distribution seen in native kidneys (average activity in medulla is nearly twice that in cortex) (*16*). Notably, in ATN rats the ^{18}F-FDG uptake emphasizes spots within the outer medulla, which is typically most affected in ischemia–reperfusion injury. Most important, the CSA-treated group (postoperative day 4) no longer showed any significant ^{18}F-FDG uptake and ^{18}F-FDG distribution was similar to that in the sTX group. Periodic acid–Schiff staining revealed that, except in the CSA treatment group (postoperative day 4), areas of intensified cellular infiltration corresponded to areas of increased ^{18}F-FDG uptake.

Histology

To estimate renal damage and infiltration for validation of ^{18}F-FDG data, we evaluated renal histology according to the ti-score as presented in Supplemental Table 1. In allografts without immunosuppressive drug treatment, we found distinct signs of acute rejection (marked glomerulitis, tubulitis, endothelialitis, and graft infiltration) in all grafts explanted on postoperative day 4, whereas these signs were absent in the grafts recovered on postoperative day 1 (Fig. 4). This finding was reflected by the ti-scoring. Although on postoperative day 1 all allografts (aTX rats) were classified as having a ti-score of 0, grafts on postoperative day 4 received a ti-score of 2–3. As demonstrated (Fig. 4; Supplemental Table 1), no histologic signs of rejection or massive infiltration were found in controls. However, renal damage according to the induced injury was present—for example, mild tubulitis or detachment of cells into the tubular lumen (ATN, acute CSA toxicity) or hyaline arteriolar

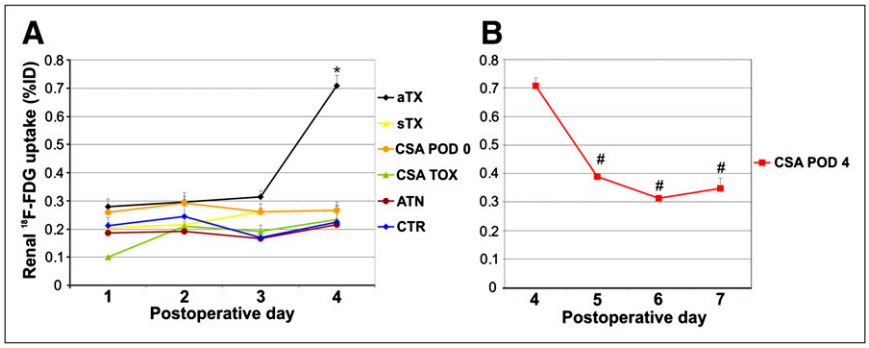

FIGURE 3. Detection of acute rejection by measurement of renal parenchyma ^{18}F-FDG uptake (%ID ± SEM) in different models for 4 d after renal injury or start of therapy (n = 5–12/model). Compared with all other models, kidneys developing acute rejection (aTX) showed significantly increased ^{18}F-FDG uptake on postoperative day 4 (A). One day after commencement of immunosuppressive therapy, ^{18}F-FDG uptake in grafts with former rejection already had significantly decreased and was no longer different from controls (B). *$P < 0.05$ vs. control. #$P < 0.05$ vs. aTX rats on postoperative day 4. CTR = control; POD = postoperative day; TOX = toxicity.

thickening (acute CSA toxicity). Interestingly, after treatment of aTX rats that had allograft rejection (postoperative day 4), signs of acute rejection tapered off. However, the clearance of infiltration was still incomplete in parts of the graft on postoperative day 7, resulting in a ti-score of 1–2.

Real-Time PCR Analysis

We used real-time PCR analysis (n = 5/group) to confirm and characterize the inflammatory cell pattern in aTX rats. Analysis of the graft leukocyte pattern revealed massive upregulation of nearly all genes of pro- and antiinflammatory cell types analyzed on aTX postoperative day 4 (Table 1) (exception: neutrophil granulocytes and T-helper cells). The cells with the highest signaling intensity were cytotoxic T cells (changes in messenger RNA [mRNA], compared with control values: CD8a, 81 ± 14; CD8b, 37 ± 8; granzyme B, 185 ± 19; $P < 0.05$) and monocytes/macrophages (ficolin B, 129 ± 11, $P < 0.05$). These cells are traditionally described as being relevant in allograft rejection (*17,18,28,29*). Upregulation of these genes (exception: neutrophil granulocytes: CD66, 3.1 ± 0.3, $P < 0.05$) was not detected on aTX postoperative day 1 (meaning that significant graft infiltration had not yet started at that time). Upregulation was also absent in isografts (sTX rats) and in the CSA group (postoperative day 0), confirming nonoccurring or successful suppression, respectively, of the rejection process by CSA treatment. CSA treatment of allograft rejection led to increased expression of proapoptotic caspase 3 (2 ± 0.1; $P < 0.05$ vs. control).

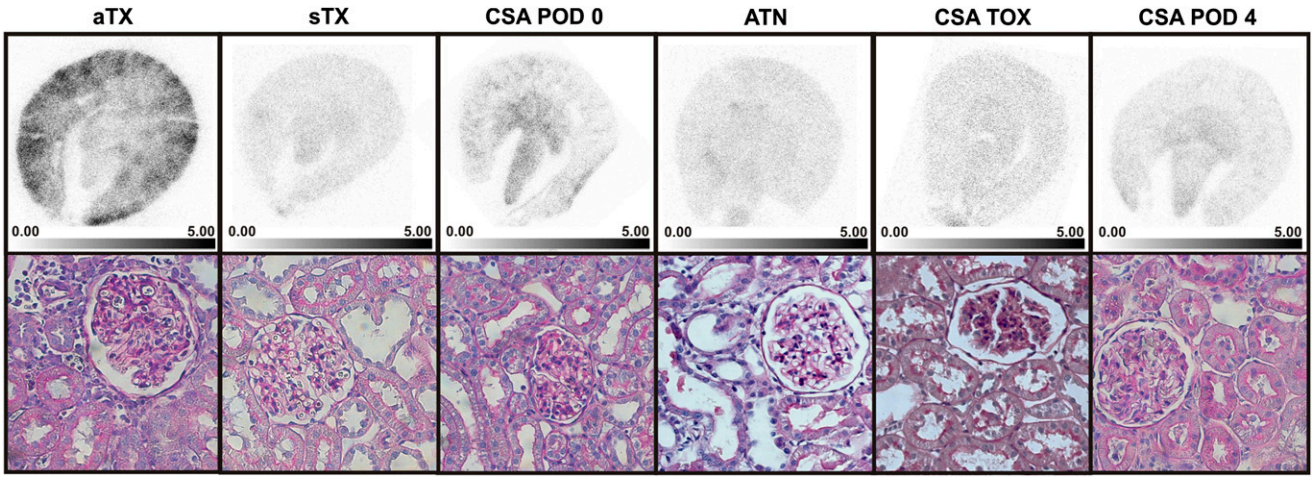

FIGURE 4. Representative autoradiographs and histologic photomicrographs 180 min after injection of 30 MBq of ^{18}F-FDG at 4 or 7 d after surgery. Although aTX graft (with acute rejection) showed intense ^{18}F-FDG activity, no significant ^{18}F-FDG accumulation occurred in sTX graft, graft with CSA treatment since postoperative day 0, kidney with ATN, kidney with CSA toxicity, or graft treated with CSA since postoperative day 4. Congruent with autoradiographic results, histologic examination (periodic acid–Schiff staining) showed signs of acute rejection, namely glomerulitis, tubulitis, endothelialitis, and graft infiltration, in aTX rats but no typical signs of rejection or massive infiltration in any other controls. Interestingly, in aTX rats treated with CSA after having developed acute rejection on postoperative day 4, signs of acute rejection tapered off. However, clearance of infiltration was still incomplete in parts of graft. POD = postoperative day; TOX = toxicity.

TABLE 1. Real-Time PCR–Based Characterization of Renal Graft Infiltration on Day 1, 4, or 7 After Surgery

Cell type	mRNA	sTX POD 4	CSA POD 0 POD 4	aTX POD 1	aTX POD 4	CSA POD 4 POD 7
T-helper cells	CD4	1.4 ± 0.1	1.9 ± 0.4	0.7 ± 0.1	1.8 ± 0.3	3.3 ± 0.8
Cytotoxic T cells	CD8a	1.2 ± 0.1	1.3 ± 0.1‡	0.3 ± 0.1	80.8 ± 13.6*†	33.8 ± 0.9‡
	CD8b	0.7 ± 0.1	1 ± 0.2‡	0.2 ± 0.1	36.6 ± 7.6*†	17.7 ± 2.0‡
Natural killer cells	CD56	1.7 ± 0.2	3 ± 0.6*	0.7 ± 0.1	0.7 ± 0.2	0.8 ± 0.2
Activation marker of cytotoxic T cells and natural killer cells	Granzyme B	0.4 ± 0.1	1.3 ± 0.2‡	0.4 ± 0.1	184.6 ± 19.2*†	54 ± 8‡
B cells, monocytes/macrophages, dendritic cells	CD40	1.6 ± 0.1	2.3 ± 0.1‡	0.2 ± 0.1	29.1 ± 3.1*†	4.2 ± 0.3‡
B cells, monocytes/macrophages	CD80	1.1 ± 0.2	1 ± 0.2‡	1.9 ± 0.4	14.2 ± 1.7*†	19.7 ± 0.2
B cells	CD20	0.5 ± 0.1	1.5 ± 0.4‡	0.3 ± 0.1	6.6 ± 1.4*†	5.4 ± 0.7
Activation marker of B cells	CD79	0.7 ± 0.1	1.9 ± 0.2*‡	0.4 ± 0.1	1.1 ± 0.1	0.9 ± 0.1
T-reg/suppressor T cells	FoxP3	1.2 ± 0.2	1.3 ± 0.1‡	0.9 ± 0.1	15.6 ± 1*†	5.2 ± 1.2c
Activation marker of monocytes/macrophages	Ficolin B	2.1 ± 0.2	4.6 ± 0.8‡	0.7 ± 0.1	128.7 ± 10.7*†	10.2 ± 2.9‡
Dendritic cells	CD83	0.6 ± 0.1	1.0 ± 0.1‡	0.4 ± 0.1	1.6 ± 0.2*†	2.1 ± 0.5
Neutrophil granulocytes	CD66	0.7 ± 0.1	1.2 ± 0.2	3.1 ± 0.3*	0.8 ± 0.6	2 ± 0.5‡

*Significantly increased relative to control ($P < 0.05$).
†Significantly increased relative to sTX ($P < 0.05$).
‡Significantly decreased relative to aTX postoperative day 4 ($P < 0.05$).
POD = postoperative day; T-reg = regulatory T cell.
Data are mean values (compared with control values, $n = 4–5$) ± SEM.

Correlation of ^{18}F-FDG to mRNA Expression of Selected Genes

We correlated ^{18}F-FDG uptake in the renal parenchyma (%ID) with mRNA expression of activity markers of monocytes/macrophages and cytotoxic T cells, which were the highest upregulated genes in aTX rats with allograft rejection (namely granzyme B and ficolin B). We found a significant correlation between these parameters ($R^2 = 0.99$ and 0.98, respectively) (Fig. 5).

Analysis of Renal Functional Parameters

To estimate renal function, blood samples were taken daily and analyzed. Before the interventions began, creatinine and BUN did not differ between groups (Table 2). Because of surgery-related damage or the toxic drug regimen, both parameters had increased significantly in all intervention groups by postoperative day 1. Recovery of renal function started immediately, leading to a continuous decrease in creatinine and BUN until postoperative day 4. Nevertheless, in comparison to all models in which the kidneys received initial damage and then recovered, aTX rats developing allograft rejection (and therefore consecutively receiving further damage) possessed the highest levels of creatinine and BUN on postoperative day 4. When CSA treatment began, creatinine and BUN initially continued to increase (CSA postoperative day 0: postoperative days 1 and 2; CSA postoperative day 4: postoperative day 5) before they decreased distinctly (Table 2). Renal functional parameters were compared with renal ^{18}F-FDG uptake to exclude decreased renal function as a potential

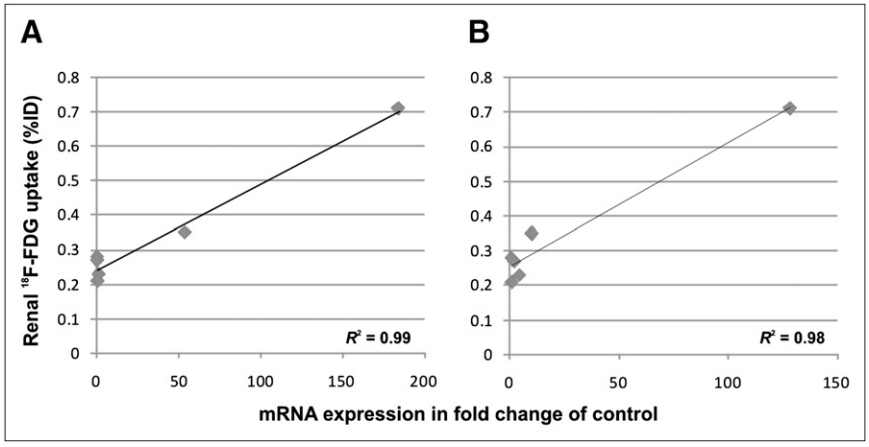

FIGURE 5. Relation of ^{18}F-FDG renal uptake to mRNA expression of activity markers of monocytes/macrophages and cytotoxic T cells, which were the highest upregulated genes in aTX rats with allograft rejection (namely granzyme B and ficolin B). We found a significant correlation between these parameters ($R^2 = 0.99$ and 0.98, respectively; $n = 6$ groups).

TABLE 2. Renal Functional Data: Serum Creatinine and BUN

Model	POD 0	POD 1	POD 2	POD 3	POD 4	POD 5	POD 6	POD 7
aTX								
Crea	0.37 ± 0.02	0.91 ± 0.06	0.78 ± 0.03	0.61 ± 0.04	0.54 ± 0.01			
BUN	22.00 ± 1.00	74.00 ± 3.00	81.00 ± 5.00	71.00 ± 7.00	55.00 ± 2.00			
CSA POD 4								
Crea	0.34 ± 0.02				0.54 ± 0.04	0.77 ± 0.07	0.73 ± 0.05	0.56 ± 0.02
BUN	25.00 ± 1.00				54.00 ± 3.00	95.00 ± 7.00	105.00 ± 5.00	82.00 ± 7.00
sTX								
Crea	0.32 ± 0.02	0.77 ± 0.03	0.60 ± 0.01	0.53 ± 0.02	0.47 ± 0.01			
BUN	24.00 ± 1.00	70.00 ± 4.00	40.00 ± 2.00	36.00 ± 1.00	37.00 ± 1.00			
CSA POD 0								
Crea	0.37 ± 0.01	1.07 ± 0.07	1.33 ± 0.15	0.53 ± 0.03	0.47 ± 0.02			
BUN	28.00 ± 1.00	93.00 ± 5.00	115.00 ± 10.00	49.00 ± 4.00	43.00 ± 1.00			
CSA toxicity								
Crea	0.28 ± 0.01	1.21 ± 0.1	0.47 ± 0.01	0.37 ± 0.01	0.36 ± 0.01			
BUN	21.00 ± 0.50	78.00 ± 4.00	52.00 ± 3.00	40.00 ± 1.00	35.00 ± 1.00			
ATN								
Crea	0.28 ± 0.01	0.67 ± 0.08	0.51 ± 0.06	0.43 ± 0.02	0.41 ± 0.01			
BUN	22.00 ± 1.00	48.00 ± 3.00	37.00 ± 5.00	32.00 ± 3.00	27.00 ± 1.00			

POD = postoperative day; Crea = serum creatinine.

cause for increased ^{18}F-FDG uptake in the renal parenchyma. ^{18}F-FDG uptake (%ID) did not correlate with creatinine (R^2 = 0.006) or BUN (R^2 = 0.05) (Fig. 6).

Accuracy of ^{18}F-FDG PET for Diagnostics of Allograft Rejection

The specificity (true-negative rate) and sensitivity of ^{18}F-FDG PET for detection of allograft rejection were calculated (Supplemental Table 3) at a cutoff value of 0.275 %ID and—at 79% and 89%, respectively—were quite high in this model.

DISCUSSION

In renal allografts, episodes of rejection are characterized by recruitment of activated leukocytes into the transplant (*17,18,29*). This is an integral part of the basic concept of the Banff classification, a commonly used score of renal rejection (*7*). Activated leukocytes strongly accumulate ^{18}F-FDG, which can be quantified by PET (*30*).

On the basis of this concept, we recently established ^{18}F-FDG PET as a noninvasive method for the detection and monitoring of renal allograft rejection using uninephrectomized rats (*16*). At present, monitoring of early treatment response is rather difficult and delayed, because up to 54% of patients with allograft rejection do not present with clinical signs (*12,13*). Biopsy as an invasive procedure usually applied in cases of persistent graft failure carries the risk of graft injury, is not feasible in patients taking anticoagulant medication, and might present false-negative results, such as when rejection is focal or patchy. Thus, the switch to a more effective therapeutic regimen could be delayed, aggravating graft failure (*12,14*). In this study, we hypothesized that ^{18}F-FDG PET is a useful noninvasive tool for assessing treatment response early, in order to translate this approach to humans in the future. Using binephrectomized rats, we applied ^{18}F-FDG PET in a renal transplant model closely mimicking the clinical situation. In this model, impairment of renal function leads to typical consequences of renal failure, such as disturbance of electrolyte and water

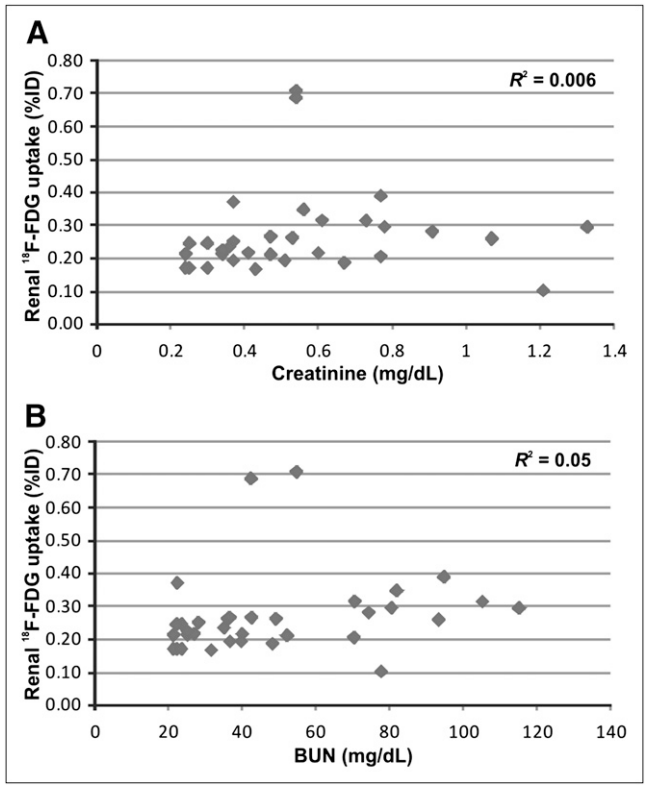

FIGURE 6. Relation of ^{18}F-FDG renal uptake to the renal functional parameters creatinine (A) and BUN (B). We found no significant correlations (R^2 = 0.006 and R^2 = 0.05, respectively; n = 34).

homeostasis or azotemia (a milieu known to affect leukocyte function) (*31*)—features that are absent in the uninephrectomized model.

First, renal ^{18}F-FDG uptake in all investigated renal injury and transplant models was quantitatively evaluated on PET images. The %ID in grafts developing rejection was significantly elevated starting on postoperative day 4, when compared with isografts or allografts under treatment with CSA. ^{18}F-FDG uptake did not increase in models developing ATN or acute CSA toxicity, which are common differential diagnoses of acute allograft rejection. Consistently, increased ^{18}F-FDG uptake in grafts undergoing rejection was already found in the lungs (*32*), liver (*33*), skin (*34*), and kidneys using a different, uninephrectomized, transplant model (*16*). Further, autoradiography showed the most intense ^{18}F-FDG signaling in allograft rejection, whereas histology revealed increased inflammatory cell infiltrates most notably in the renal cortex of allograft rejection. In all control models used, ^{18}F-FDG signal intensity was on the level of native kidneys whereas inflammation was absent, concentrated to small and distinct areas (ATN: spots in the outer medulla), or classified as mild (<10% of parenchyma). These results were supported by real time PCR analysis of proinflammatory cell markers within the kidneys. In control and sTX rats, we could not detect relevant amounts of mRNA of proinflammatory cells, whereas aTX rats on postoperative day 0 (the rats treated with CSA since the transplantation procedure) presented with very low levels of T-cell, B-cell, and monocyte/macrophage marker mRNA on postoperative day 4. However, the ti-score was still 0. Interestingly, on postoperative day 1 in aTX rats without an immunosuppressive regimen, the mRNA of proinflammatory cells had not yet increased (a ti-score of 0), whereas we found high expression of marker mRNA from cytotoxic T cells and monocytes/macrophages and lower but still significant levels of B cells, regulatory T cells, and dendritic cells on postoperative day 4 (a ti-score of 2–3). Because granzyme B and ficolin B gene expression were highly upregulated on postoperative day 4, one can assume that cytotoxic and regulatory T cells and monocytes/macrophages were highly activated (*28*), as is commonly found during allograft rejection (*29*). As expected, our findings suggest that ^{18}F-FDG detects changes in renal glucose metabolism consistent with activated inflammatory infiltrates occurring in renal allografts. Notably, we found a significant correlation between the mRNA expression of granzyme B and ficolin B (activation marker genes of cytotoxic T cells and monocytes/macrophages) and ^{18}F-FDG in all groups measured (Fig. 5).

Regarding renal functional data, creatinine and BUN had increased in all intervention groups by postoperative day 1. Recovery of renal function started immediately, leading to a continuous decrease of creatinine and BUN until postoperative day 4, with the highest levels in aTX rats developing allograft rejection (and therefore consecutively receiving further damage). Hence, ^{18}F-FDG PET correctly diagnosed allograft rejection in rats with decreasing creatinine and BUN values on postoperative day 4, pointing to the capability of PET to detect allograft rejection early.

Morath et al. performed protocol biopsies on patients with delayed graft function 1 wk after transplantation *(9)*. Allograft rejection was confirmed in 18% of patients with delayed graft function, compared with only 4% of patients with early graft function. Of allograft rejection episodes in patients with delayed graft function, 50% had remained clinically undiagnosed and were revealed only by the protocol biopsies, whereas allograft rejection would have remained undiagnosed on clinical grounds in all patients with delayed graft function who required dialysis. Similar results were reported by Shapiro et al. (*35*). Every fifth patient with normal or improving renal function had borderline histopathologic findings, and 1 of 4 had frank acute tubulitis (Banff 1A to 2A). Similar observations were published by Rush, who performed protocol biopsies 3 mo after transplantation (*8*). Thus, it was postulated that more than 50% of the allograft rejection episodes are subclinical at some time after renal transplantation without acute impairment of renal function. Therefore, we believe that ^{18}F-FDG PET is a valuable diagnostic tool to avoid unnecessary biopsies, mainly in patients with inconspicuous laboratory results and clinical evolution.

Second, renal ^{18}F-FDG uptake in aTX rats treated with CSA remained low and stable during treatments, suggesting that ^{18}F-FDG PET can be used to monitor the efficacy of immunosuppressive therapy as a noninvasive method, in contrast to biopsy. However, there are other methods, such as assessment of renal serum parameters, for evaluation of transplant function. To enlarge the potential use of ^{18}F-FDG PET for treatment follow-up, we included a group of rats that developed allograft rejection, which was treated by CSA since postoperative day 4. Notably, ^{18}F-FDG signaling decreased only 24 h after commencement of therapy (postoperative day 5) to levels nearly those of controls and stayed at these levels until the end of follow-up. Analysis of functional renal parameters revealed that creatinine and BUN decreased 24 and 48 h later (postoperative days 6–7), respectively. Moreover, renal histology showed a degree of infiltration that was still relevant (ti-score of 1–2) in these grafts on postoperative day 7, potentially leading to the diagnosis of active, therapy-refractory allograft rejection. However, in our model these cells responded to treatment as confirmed by PCR analysis of gene expression profile, such as decreased expression of CD8a/b and ficolin B and increased expression of pro-apoptotic caspase 3. Therefore, detection of treatment response was 24–48 h earlier when ^{18}F-FDG PET was applied. Consistently, Lopes de Souza et al. used ^{99m}Tc-labeled mononuclear leukocytes for detection of renal allograft rejection in humans. In their study, scintigraphy detected allograft rejection on postoperative day 5 (but not on postoperative day 1), which was around 2–3 d before clinical manifestations (*36*). The fact that ^{18}F-FDG PET correctly diagnosed treatment

response in rats with increasing creatinine and BUN values points to the capability of PET to detect early treatment response.

These findings might yield consequences for the management of patients undergoing allograft rejection, because it might be possible to react to treatment response or nonresponse earlier. In the case of treatment response, one might reduce immunosuppressive drug doses and thereby limit their side-effects, because a successful response to therapy is classically defined as a relative serum creatinine concentration no more than 110% of the concentration on the day of diagnosed rejection (day 0) and returning to the day 0 value or less within 5 d of therapy (*12*). Even more important, in the case of treatment-unresponsive allograft rejection, escalation of the immunosuppressive regimen can start earlier. Earlier escalation might prevent graft damage by shortening allograft rejection episodes. At present, steroid-resistant rejection—an allograft rejection episode that has been treated with up to 1 g of methylprednisolone and in which the creatinine concentration fails to stabilize or lessen after 3 d of therapy—is diagnosed late (*12*).

Two potential problems in applying ^{18}F-FDG PET to the clinical setting should be addressed. Urinary excretion of the tracer might induce artificially high renal ^{18}F-FDG uptake. Thus, the renal pelvis was carefully excluded from the measurements. Various techniques such as hydration or administration of diuretics have been used to improve the diagnostic yield of PET by increasing diuresis for dilution of urinary ^{18}F-FDG (*37*). In view of the results of preliminary dynamic ^{18}F-FDG investigations, we chose late acquisitions 3 h after injection to reduce the tracer concentration in the urine during the PET scan. The impact of renal function on ^{18}F-FDG uptake seems to be minimal in our model because ^{18}F-FDG uptake did not correlate with creatinine and BUN (Fig. 6). Moreover, in a previous study we did not find a correlation between fluoride clearance (a method for noninvasive assessment of renal function (*21*)) and ^{18}F-FDG uptake (*16*). Nevertheless, significant renal ^{18}F-FDG accumulation was present in allograft rejection only, whereas renal insufficiency was observed in other groups, too (Table 2). However, we cannot exclude the possibility that a part of the PET signal might refer to excreted ^{18}F-FDG. When renal biopsy needs to be performed despite suspected allograft rejection, such as in cases of patchy rejection patterns, ^{18}F-FDG PET might help to determine the appropriate location.

The second problem is the inevitably impaired specificity in diagnosing allograft rejection: although ^{18}F-FDG uptake certainly detects enhanced metabolic activity, ^{18}F-FDG uptake is not disease-specific. Thus, graft infection or tumors might also cause ^{18}F-FDG uptake on PET. However, if clinical symptoms pointing to malignancy (e.g., weight loss or night sweating) or to urinary tract infection (e.g., fever or dysuria) are present, target-orientated additional diagnostics such as ultrasound, blood tests, or urine tests should be applied.

CONCLUSION

We propose the use of ^{18}F-FDG PET for the follow-up of patients undergoing renal transplantation to allow early diagnosis of allograft rejection and early evaluation of treatment response and to assist in the differential diagnosis of ATN and acute CSA toxicity.

ACKNOWLEDGMENTS

This study was supported in part by the Rolf-Dierichs-Foundation, the Interdisciplinary Centre for Clinicial Research (IZKF, Core Unit SmAP), and the Deutsche Forschungsgemeinschaft (SFB 656 C7), Münster, Germany. We thank Anne Kanzog, Ute Neugebauer, Sandra Schröer, Irmgard Hoppe, and Sven Hermann for providing excellent technical assistance, and we thank Daniel Burkert and Sven Fatum for producing the radiotracers.

REFERENCES

1. Matas AJ, Gillingham KJ, Payne WD, Najarian JS. The impact of an acute rejection episode on long-term renal allograft survival (t1/2). *Transplantation.* 1994;57:857–859.
2. Meier-Kriesche HU, Ojo AO, Hanson JA, et al. Increased impact of acute rejection on chronic allograft failure in recent era. *Transplantation.* 2000;70:1098–1100.
3. Opelz G, Dohler B. Influence of time of rejection on long-term graft survival in renal transplantation. *Transplantation.* 2008;85:661–666.
4. Chapman JR, O'Connell PJ, Nankivell BJ. Chronic renal allograft dysfunction. *J Am Soc Nephrol.* 2005;16:3015–3026.
5. Hariharan S, Johnson CP, Bresnahan BA, Taranto SE, McIntosh MJ, Stablein D. Improved graft survival after renal transplantation in the United States, 1988 to 1996. *N Engl J Med.* 2000;342:605–612.
6. Massy ZA, Guijarro C, Wiederkehr MR, Ma JZ, Kasiske BL. Chronic renal allograft rejection: immunologic and nonimmunologic risk factors. *Kidney Int.* 1996;49:518–524.
7. Racusen LC, Solez K, Colvin RB, et al. The Banff 97 working classification of renal allograft pathology. *Kidney Int.* 1999;55:713–723.
8. Rush D. Protocol transplant biopsies: an underutilized tool in kidney transplantation. *Clin J Am Soc Nephrol.* 2006;1:138–143.
9. Morath C, Ritz E, Zeier M. Protocol biopsy: what is the rationale and what is the evidence? *Nephrol Dial Transplant.* 2003;18:644–647.
10. El-Mekresh M, Osman Y, li-El-Dein B, El-Diasty T, Ghoneim MA. Urological complications after living-donor renal transplantation. *BJU Int.* 2001;87:295–306.
11. Schwarz A, Hiss M, Gwinner W, Becker T, Haller H, Keberle M. Course and relevance of arteriovenous fistulas after renal transplant biopsies. *Am J Transplant.* 2008;8:826–831.
12. Guttmann RD, Soulillou JP, Moore LW, et al. Proposed consensus for definitions and endpoints for clinical trials of acute kidney transplant rejection. *Am J Kidney Dis.* 1998;31(6, suppl 1)S40–S46.
13. Guttmann RD, Soulillou JP. Definitions of acute rejection and controlled clinical trials in the medical literature. *Am J Kidney Dis.* 1998;31(6, suppl 1)S3–S6.
14. Becker YT, Becker BN, Pirsch JD, Sollinger HW. Rituximab as treatment for refractory kidney transplant rejection. *Am J Transplant.* 2004;4:996–1001.
15. Meller J, Sahlmann CO, Scheel AK. ^{18}F-FDG PET and PET/CT in fever of unknown origin. *J Nucl Med.* 2007;48:35–45.
16. Reuter S, Schnöckel U, Schröter R, et al. Non-invasive imaging of acute renal allograft rejection in rats using small animal ^{18}F-FDG-PET. *PLoS ONE.* 2009;4:e5296.
17. Gallon L, Gagliardini E, Benigni A, et al. Immunophenotypic analysis of cellular infiltrate of renal allograft biopsies in patients with acute rejection after induction with alemtuzumab (Campath-^{1}H). *Clin J Am Soc Nephrol.* 2006;1:539–545.
18. Sarwal M, Chua MS, Kambham N, et al. Molecular heterogeneity in acute renal allograft rejection identified by DNA microarray profiling. *N Engl J Med.* 2003;349:125–138.
19. Edemir B, Reuter S, Borgulya R, et al. Acute rejection modulates gene expression in the collecting duct. *J Am Soc Nephrol.* 2008;19:538–546.

20. Reuter S, Velic A, Edemir B, et al. Protective role of NHE-3 inhibition in rat renal transplantation undergoing acute rejection. *Pflugers Arch.* 2008;456: 1075–1084.
21. Schnöckel U, Reuter S, Stegger L, et al. Dynamic ^{18}F-fluoride small animal PET to noninvasively assess renal function in rats. *Eur J Nucl Med Mol Imaging.* 2008;35:2267–2274.
22. Schäfers KP, Reader AJ, Kriens M, Knoess C, Schober O, Schafers M. Performance evaluation of the 32-module quadHIDAC small-animal PET scanner. *J Nucl Med.* 2005;46:996–1004.
23. Reader AJ, Ally S, Bakatselos F. One-pass list-mode EM algorithm for high resolution 3D PET image reconstruction into large arrays. *IEEE Trans Nucl Sci.* 2002;49:693–699.
24. Solez K, Colvin RB, Racusen LC, et al. Banff 07 classification of renal allograft pathology: updates and future directions. *Am J Transplant.* 2008;8: 753–760.
25. Sis B, Sarioglu S, Celik A, et al. Renal medullary changes in renal allograft recipients with raised serum creatinine. *J Clin Pathol.* 2006;59:377–381.
26. Livak KJ, Schmittgen TD. Analysis of relative gene expression data using real-time quantitative PCR and the 2(-Delta Delta C(T)) method. *Methods.* 2001;25:402–408.
27. Kaim AH, Weber B, Kurrer MO, Gottschalk J, Von Schulthess GK, Buck A. Autoradiographic quantification of ^{18}F-FDG uptake in experimental soft-tissue abscesses in rats. *Radiology.* 2002;223:446–451.
28. Edemir B, Kurian SM, Eisenacher M, et al. Activation of counter-regulatory mechanisms in a rat renal acute rejection model. *BMC Genomics.* 2008;9:71.
29. Nickeleit V, Andreoni K. Inflammatory cells in renal allografts. *Front Biosci.* 2008;13:6202–6213.
30. Pellegrino D, Bonab AA, Dragotakes SC, Pitman JT, Mariani G, Carter EA. Inflammation and infection: imaging properties of ^{18}F-FDG-labeled white blood cells versus ^{18}F-FDG. *J Nucl Med.* 2005;46:1522–1530.
31. Reuter S, Bangen P, Edemir B, et al. The HSP72 stress response of monocytes from patients on haemodialysis is impaired. *Nephrol Dial Transplant.* 2009;24: 2838–2846.
32. Hoff SJ, Stewart JR, Frist WH, et al. Noninvasive detection of heart transplant rejection with positron emission scintigraphy. *Ann Thorac Surg.* 1992;53:572–577.
33. Tsuji AB, Morita M, Li XK, et al. ^{18}F-FDG PET for semiquantitative evaluation of acute allograft rejection and immunosuppressive therapy efficacy in rat models of liver transplantation. *J Nucl Med.* 2009;50:827–830.
34. Heelan BT, Osman S, Blyth A, Schnorr L, Jones T, George AJ. Use of 2-[^{18}F] fluoro-2-deoxyglucose as a potential agent in the prediction of graft rejection by positron emission tomography. *Transplantation.* 1998;66:1101–1103.
35. Shapiro R, Randhawa P, Jordan ML, et al. An analysis of early renal transplant protocol biopsies: the high incidence of subclinical tubulitis. *Am J Transplant.* 2001;1:47–50.
36. Lopes de Souza SA, Barbosa da Fonseca LM, Torres GR, et al. Diagnosis of renal allograft rejection and acute tubular necrosis by ^{99m}Tc-mononuclear leukocyte imaging. *Transplant Proc.* 2004;36:2997–3001.
37. Anjos DA, Etchebehere EC, Ramos CD, Santos AO, Albertotti C, Camargo EE. ^{18}F-FDG PET/CT delayed images after diuretic for restaging invasive bladder cancer. *J Nucl Med.* 2007;48:764–770.